Nonnormal Perturbation Growth of Pure Thermohaline Circulation Using a 2D Zonally Averaged Model

JULIE ALEXANDER

School of Earth and Ocean Sciences, University of Victoria, Victoria, British Columbia, Canada

ADAM H. MONAHAN

School of Earth and Ocean Sciences, University of Victoria, Victoria, British Columbia, and Canadian Institute for Advanced Research, Earth Systems Evolution Program, Toronto, Ontario, Canada

(Manuscript received 29 May 2007, in final form 7 August 2008)

ABSTRACT

Generalized linear stability theory is used to calculate the optimal initial conditions that result in transient amplification of the thermohaline circulation (THC) in a zonally averaged single-basin ocean model. The eigenmodes of the tangent linear model verify that the system is asymptotically stable, but the nonnormality of the system permits the growth of perturbations for a finite period through the interference of nonorthogonal eigenmodes. It is found that the maximum amplification of the THC anomalies occurs after 6 yr with both the thermally and salinity-driven components playing major roles in the amplification process. The transient amplification of THC anomalies is due to the constructive and destructive interference of a large number of eigenmodes, and the evolution over time is determined by how the interference pattern evolves. It is found that five of the most highly nonnormal eigenmodes are critical to the initial cancellation of the salinity and temperature contributions to the THC, while 11 oscillating modes with decay time scales ranging from 2 to 6 yr are the major contributors at the time of maximum amplification. This analysis demonstrates that the different dynamics of salinity and temperature anomalies allow the dramatic growth of perturbations to the THC on relatively short (interannual to decadal) time scales.

1. Introduction

The thermohaline circulation (THC) is an important feature of the global climate system, transporting a large amount of heat to the high-latitude North Atlantic [approximately 1×10^{15} W according to Ganachaud and Wunsch (2000)]. Evidence from general circulation model (GCM) simulations (Manabe and Stouffer 1999) and paleoproxies (Clark et al. 2002; O'Hare et al. 2005) suggest that variations in the intensity of the THC are likely to change the climate significantly. The main time scales and mechanisms of variability of the THC are not well known and considerable uncertainty remains in the stability of the present THC. Simulations with climate models can provide useful information regarding the dominant time scales of THC fluctuations, both in terms of internal variability and adjustment to external forcing. In a study by Vellinga and Wood (2002), the third climate configuration of the Met Office Unified Model (HadCM3) ocean–atmosphere general circulation model was used to study climate feedbacks after a major disruption of the THC. In this study, the THC was made to collapse by applying strong freshwater forcing to the top layers of the North Atlantic. After about 100 yr, the model's THC had largely recovered and most climatic anomalies had disappeared. The rapid growth of perturbations in a system is of considerable theoretical interest because it may be a precursor to a large-scale event. Finding the spatial structure of the optimal salinity and temperature perturbations that lead to the maximum response of the THC also gives insight into the dynamical mechanisms that may be particularly effective for triggering disruptive events.

In addition, there is evidence gathered from paleoclimate data that the climate system of the earth has undergone dramatic and abrupt changes in the past. High-resolution records indicate that large-amplitude

Corresponding author address: Julie Alexander, School of Earth and Ocean Sciences, University of Victoria, P.O. Box 3055, STN CSC, Victoria, BC V8P 5C2, Canada.
E-mail: jalexndr@uvic.ca

DOI: 10.1175/2008JPO3847.1

changes have occurred on millennial time scales, with transitions occurring on time scales of decades (Clark et al. 2002; Rahmstorf 2002). There is a possibility (albeit slight) that future changes of the climate system may exhibit similar nonlinear behavior (Meehl et al. 2007); such changes cannot be easily extrapolated from ongoing observed changes. A characteristic of nonlinear behavior, such as the collapse of the global THC, is very low predictability. Therefore, it is important to increase our understanding of the variability of the THC at points both near and far from nonlinear thresholds. Changes in the thermohaline circulation would seriously affect the climate in eastern North America and western and central Europe, as well as impact the ocean's biogeochemical cycles and future sea level.

Paleoclimate evidence suggests that the THC has been remarkably stable over the past 10 000 yr (McManus et al. 2004) with present-day variability estimated to be between 5% and 10% of the mean transport (Pasquero and Tziperman 2004), suggesting that the present-day THC can be characterized as a stable linear dynamic system that may be excited by stochastic ''weather'' forcing (Griffies and Tziperman 1995; Pasquero and Tziperman 2004). This statement implies that the eigenmodes of the linearized dynamics, $dx/dt = \mathbf{A}x$, must all have exponentially decaying amplitudes, so any initial perturbation must eventually decay, where x is the perturbation state vector (anomalies around some steady-state solution) and $\mathbf{A}$ is the linearized dynamical operator. Traditional linear stability theory focuses on the eigenmodes of the tangent linear operator $\mathbf{A}$ and searches for perturbations that grow exponentially with time (e.g., Pedlosky 1987). If all of the eigenvalues of $\mathbf{A}$ are negative, then the system is asymptotically stable and all small perturbations applied to the steady state will decay to zero as $(t \to \infty)$ If $\mathbf{A}$ possesses at least one growing eigenmode, then the tangent linear dynamical system is considered to be asymptotically unstable. However, this view of stability focuses on the long-term behavior of the linear system; more complex behavior is possible over finite times. If $\mathbf{A}$ is normal, that is, it commutes with its adjoint, then its eigenmodes are orthogonal and no perturbation can grow faster than the most unstable eigenmode (Moore et al. 2003). However, if $\mathbf{A}$ is nonnormal (does not commute with its adjoint), it is possible for perturbations to grow more rapidly than the most unstable eigenmode. In particular, if all of the eigenmodes of a nonnormal system are asymptotically stable, it is still possible for the perturbation vector in a nonnormal system to undergo a transient growth at any given finite time before its eventual decay (Farrell and Ioannou 1996). This transient growth is due to the linear interference of the nonorthogonal eigenmodes of the matrix $\mathbf{A}$.

In the Euclidean norm, the adjoint of a matrix is the Hermitian transpose, but applications often require using a norm other than the Euclidean. Farrell and Ioannou (1996) show that by an appropriate transformation of dynamical operators, the analysis can proceed as in the Euclidean norm with the implication that it is possible to render an operator normal by choosing an appropriate norm. However, such a norm is usually not based on physical grounds and it is very unlikely that an operator that is nonnormal in the Euclidean norm will become normal under a physically based norm.

The linear superposition of eigenmodes that yields the fastest-growing perturbation with respect to a given norm and time interval is called an ''optimal perturbation'' (Farrell and Ioannou 1996). Because optimality is defined relative to a particular norm, the optimal perturbations are norm dependent (in contrast to the normal modes). By studying optimal perturbations, disturbances that grow rapidly with respect to a given norm can be identified and attention can be drawn to dynamically interesting parts of the flow. As most geophysical systems are in fact nonnormal, the techniques of generalized stability theory have been applied to a variety of problems. It has been shown in numerous studies (e.g., Farrell and Ioannou 1993a,b, 1995, 1996; DelSole and Farrell 1995; Aiken et al. 2002; Moore et al. 2003; Moore et al. 2002) that a nonnormal system responds differently to steady forcing than does a normal system.

A number of studies have investigated the nonnormal dynamics of the THC (Lohmann and Schneider 1999; Tziperman and Ioannou 2002; Zanna and Tziperman 2005; Sevellec et al. 2007, Tziperman et al. 2008). This study investigates the transient amplification of the THC using an ocean circulation model with a more sophisticated representation of the ocean dynamics than that used in previous studies. A hierarchy of climate models has been developed to study the structure and variability of the THC (Weaver et al. 1999; Monahan et al. 2008). Although simple box models provide a means of exploring basic physical processes of the THC [e.g., Stommel (1961), who used such a model to demonstrate that it is possible for the THC to have multiple equilibria for identical surface forcing], they have severe limitations. Considering the ocean as large, well-mixed reservoirs prevents modeling of deep-water formation in specific areas and the subsequent upwelling through the stratified thermocline.

The model used in this study is the zonally averaged ocean-only model of Stocker and Wright (1991), Wright and Stocker (1991), and Wright et al. (1995). Unlike the

box models considered in Lohmann and Schneider (1999), Tziperman and Ioannou (2002), and Zanna and Tziperman (2005), this model is on a spherical domain, takes into account the rotation of the earth, and employs a direct representation of the momentum budget. Although Sevellec et al. (2007) use a similar 2D zonally averaged model for their study, there are a number of differences between their study and ours. In particular, they consider only surface salinity perturbations and neglect temperature perturbations. In the configuration considered in this study, this model simulates the THC as driven by buoyancy forcing alone; the effects of surface wind forcing have been neglected. In this sense, this study focuses on the dynamics of pure thermohaline circulation.

The paper is organized as follows: in section 2, the model is described. The linear theory is presented in section 3. Section 4 describes the optimal initial conditions and the evolution of the optimal perturbation to the THC. A discussion and comparison to previous studies are given in section 5. Conclusions follow in section 6.

2. Model description

The ocean model considered in this study is a 2D zonally averaged model developed by Wright and Stocker (1991) as a model of reduced complexity for the study of the structure and variability of the large-scale THC. This model, which we shall refer to as the WS model, has been shown to be capable of reproducing the major features of the present-day THC (Stocker and Wright 1991; Wright and Stocker 1991; Wright et al. 1995). Numerous studies have used this model to investigate the mechanisms involved in the variability of the THC, the existence of multiple equilibria, and transitions between these equilibria (e.g., Aeberhardt et al. 2000; Stocker et al. 1992a,b; Schmittner and Stocker 2001; Schmittner and Weaver 2001; Knutti and Stocker 2002).

The WS model has also been shown to be sensitive to changes in internal parameters in a manner similar to OGCMs (Wright and Stocker 1991; Knutti et al. 2000). The sensitivity of the THC to switches between restoring and mixed boundary conditions and the amounts, rates, and locations of freshwater input required to trigger a conveyor shutdown have been extensively investigated using the WS model (Stocker and Wright 1991; Wright and Stocker 1991; Stocker et al. 1992a,b; Vellinga 1996) as have the possible impacts of global warming on the atmosphere–ocean system (Schmittner and Stocker 1999; Stocker et al. 1994; Stocker and Wright 1996). Resonant, stable, centennial-scale oscillations about the steady state in a randomly forced WS model were observed by Schmidt and Mysak (1996). This earlier study focused on the eigenstructure of the linearized dynamics and did not consider transient amplification of THC anomalies.

The state variables of the WS model are temperature and salinity. The model dynamics follow from the Boussinesq equations formulated on a spherical coordinate frame, zonally averaged between the east and west boundaries of the ocean basin of angular width $\Delta\Lambda$. In the following equations, all state variables are zonally averaged.

The prognostic equations are the conservation of energy and salt expressed as advection–diffusion equations:

$$\frac{\partial T}{\partial t} + \frac{1}{c}\frac{\partial}{\partial \phi}\left(\frac{cv}{a}T\right) + \frac{\partial}{\partial z}(wT) = \frac{1}{c}\frac{\partial}{\partial \phi}\left(\frac{cK_H}{a^2}\frac{\partial T}{\partial \phi}\right) + \frac{\partial}{\partial z}\left(K_V\frac{\partial T}{\partial z}\right) \quad (1)$$

and

$$\frac{\partial S}{\partial t} + \frac{1}{c}\frac{\partial}{\partial \phi}\left(\frac{cv}{a}S\right) + \frac{\partial}{\partial z}(wS) = \frac{1}{c}\frac{\partial}{\partial \phi}\left(\frac{cK_H}{a^2}\frac{\partial S}{\partial \phi}\right) + \frac{\partial}{\partial z}\left(K_V\frac{\partial S}{\partial z}\right). \quad (2)$$

Horizontal momentum balance is represented by geostrophic balance without horizontal or vertical diffusion of momentum:

$$2s\Omega u = -\frac{1}{\rho_* a}\frac{\partial p}{\partial \phi} \quad (3)$$

and

$$-2s\Omega v = -\frac{1}{\rho_* ac}\frac{\Delta p}{\Delta \Lambda}. \quad (4)$$

The assumption of balance does not imply that momentum diffusion is unimportant in determining zonally averaged oceanic conditions. In the present formulation, momentum diffusion is implicitly taken into consideration by defining a relationship between the east–west pressure difference and the north–south density gradient, as will be discussed below. Vertical momentum balance is represented by hydrostatic equilibrium,

$$\frac{\partial p}{\partial z} = -\rho g, \quad (5)$$

and mass conservation is represented by the continuity equation

$$\frac{1}{ac}\frac{\partial}{\partial \phi}(cv) + \frac{\partial}{\partial z}w = 0. \quad (6)$$

A linearized equation of state is used to close the system:

$$\rho = \rho_*[1 - \alpha(T - T_0) + \beta(S - S_0)], \tag{7}$$

where $\alpha = 0.223\ \mathrm{K}^{-1}$, $\beta = 0.796\ \mathrm{psu}^{-1}$, and $\rho_* = 1027\ \mathrm{kg\ m}^{-3}$ is the constant reference density. In the above equations, ϕ is the latitude; $s = \sin\phi$, $c = \cos\phi$ and z are the vertical coordinates, increasing from $-H$ at the bottom to zero at the surface; u, v and w are the zonally averaged horizontal and vertical velocity components; T, S, ρ, and P denote zonally averaged potential temperature referenced to the surface, salinity, in situ density, and pressure; Ω and a are the angular velocity and radius of the earth, and g is the acceleration due to gravity. The constant horizontal and vertical diffusion coefficients are, respectively, $K_H = 1.0 \times 10^3\ \mathrm{m^2\ s^{-1}}$ and $K_V = 1.0 \times 10^{-4}\ \mathrm{m^2\ s^{-1}}$. For this study, the model is a single Boussinesq ocean basin with a uniform depth of 5000 m and a constant angular width of 60° in the Northern Hemisphere only, discretized to 20 vertical layers and 20 latitudes.

It is not possible to determine the east–west zonally averaged pressure gradient $\Delta p/\Delta\Lambda$ from the model equations given above. Wright and Stocker (1991) parameterized this pressure gradient in terms of the north–south density gradient. This parameterization guarantees that $u, v = 0$ at the lateral boundaries, and it can be approximated by the relation

$$\frac{\Delta p}{\Delta\Lambda} = -\varepsilon \sin(2\phi)\frac{\partial p}{\partial \phi}, \tag{8}$$

where ε is a closure parameter that depends on the width of the basin. Wright and Stocker (1991) provide a discussion of the test of the validity of this parameterization. This closure scheme was developed for models with no wind stress. To simplify the analysis, a value of $\varepsilon = 0.45$ (as used in Wright and Stocker 1991) was chosen for this study.

No-flux conditions are specified for T and S at solid boundaries:

$$\frac{\partial T}{\partial s} = \frac{\partial T}{\partial z} = \frac{\partial S}{\partial s} = \frac{\partial S}{\partial z} = 0. \tag{9}$$

Furthermore, rigid boundaries are assumed: $v = 0$ at the northern and southern walls and $w = 0$ at the top and bottom of the basin. The vertical flux of heat and salt at the surface are parameterized by

$$-K_V T_z = \frac{H_M}{\Gamma_T}(T - T_*) \tag{10}$$

and

$$-K_V S_z = \frac{H_M}{\Gamma_S}(S - S_*), \tag{11}$$

where $H_M = 50$ m is the depth of the surface layer, Γ_T is the relaxation time scale for temperature, and Γ_S is the relaxation time scale for salt. Surface temperature and salinity are restored to observed fields of annual mean temperature T_* and salinity S_* as compiled by Levitus (1982). Plots of S_* and T_* as a function of latitude in the Northern Hemisphere are shown in Figs. 1a,b, respectively. The relaxation times chosen for this study are $\Gamma_T = 30$ and $\Gamma_S = 120$ days.

Finally, the meridional overturning streamfunction Ψ is defined by

$$v = -\frac{1}{c}\frac{\partial \Psi}{\partial z} \tag{12}$$

and

$$w = -\frac{1}{ac}\frac{\partial \Psi}{\partial \phi}, \tag{13}$$

with $\Psi = 0$ at the top and bottom of the basin for all latitudes.

The solution procedure is as follows: the temperature and salinity fields are calculated using forward time differencing, and numerical diffusion associated with the advective terms is reduced using the method described in Wright and Stocker (1991). The density field is determined by the linear equation of state, and from this the streamfunction and velocity fields can be calculated as described in Wright and Stocker (1991).

Static instabilities are removed using the convection scheme described in Wright and Stocker (1991). This is an efficient mixing scheme that parameterizes small-scale motions not resolved by the model. Unstable stratification is removed by determining the top and bottom cells of unstable parts of the water column and setting the temperature and salinity to the volume-weighted mean over this region. The effect of convection is to reduce vertical density gradients and mix down any positive density anomalies on very short time scales. For all time steps of the full nonlinear model, the vertical water columns were swept four times to remove static instabilities.

3. Linear theory

In this paper the techniques of generalized linear stability theory (Farrell and Ioannou 1996) are used to calculate the linear perturbations that lead to the most rapid growth of THC anomalies. The system of

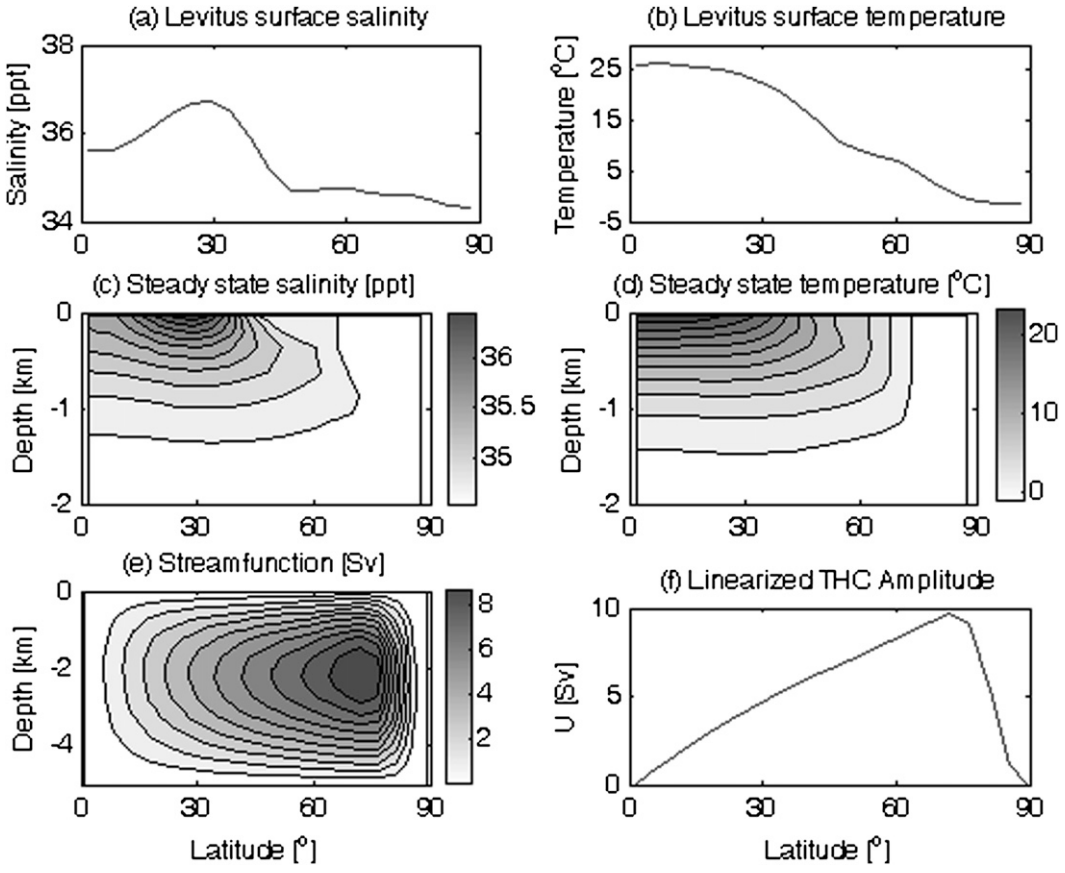

FIG. 1. Surface forcing fields of (a) salinity and (b) temperature from Levitus (1982), and steady-state fields after 12 000-yr spinup, (c) salinity, (d) temperature, (e) streamfunction, and (f) THC amplitude.

governing equations may be written in terms of a nonlinear operator **N**:

$$\frac{d\mathbf{P}(t)}{dt} = \mathbf{N}[\mathbf{P}(t)], \tag{14}$$

where **P** is the state vector of the system consisting of the temperature and salinity at each grid point. If a perturbation $\mathbf{P}'$ is added to the steady-state solution, then the perturbation evolution is described by

$$\frac{d\mathbf{P}'}{dt} = \left(\frac{d\mathbf{N}}{d\mathbf{P}}\right)_{\bar{\mathbf{P}}} \mathbf{P}' + \text{higher order terms} \approx \mathbf{A}\mathbf{P}', \tag{15}$$

assuming that $\mathbf{P}'$ is sufficiently small so that terms of quadratic and higher order in $\mathbf{P}'$ are negligible compared to $\mathbf{A}\mathbf{P}'$.

The tangent linear operator **A**, which represents the linearized model equations, is defined as

$$\mathbf{A} = \left(\frac{d\mathbf{N}}{d\mathbf{P}}\right)_{\bar{\mathbf{P}}}. \tag{16}$$

A time-independent steady state is used to simplify the analysis and dynamical interpretation of the system. In this case, the system is autonomous and its eigenmodes evolve exponentially in time. The solution of the tangent linear system is

$$\mathbf{P}'(t) = e^{At}\mathbf{P}'(t=0) = \mathbf{B}(t,0)\mathbf{P}'(0), \tag{17}$$

where the matrix $\mathbf{B}(t,0) = e^{At} \equiv \mathbf{B}(t)$ is known as the propagator of the system because it advances the state vector forward in time and $\mathbf{P}'(0) \equiv \mathbf{P}'_0$ is the perturbation state vector at $t = 0$.

4. Optimal initial conditions

a. Structure and evolution

The full nonlinear model is started from rest with the ocean at a uniform temperature of 4°C and salinity of 35 ppt, and it is run to steady state for 12 000 yr under the restoring boundary conditions described in Eqs. (10) and (11). The steady-state salinity field, temperature field, and streamfunction reached by the full nonlinear

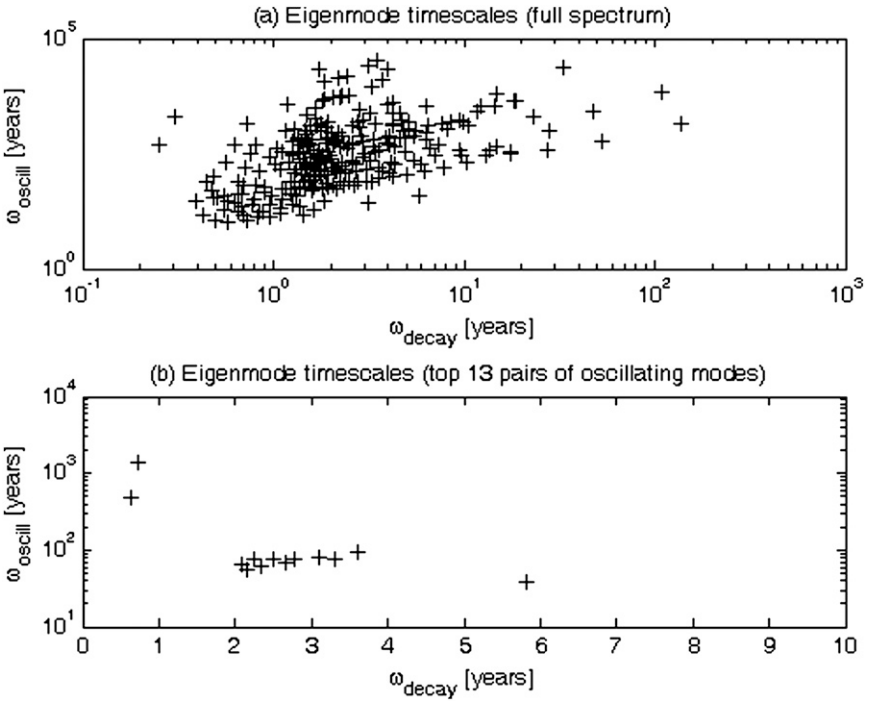

FIG. 2. (a) Oscillation time scale vs decay time scale for the eigenmodes of the linear tangent matrix **A** and (b) oscillation time scale vs decay time scale for the top 13 pairs of oscillating eigenmodes responsible for the transient amplification of the THC amplitude. Each eigenmode with a nonzero oscillation time scale has a corresponding complex conjugate whose oscillation time scale is the negative of the original oscillation time scale. Not shown in (b) are the three purely decaying modes that are important contributors to the transient amplification whose decay time scales are 0.65, 0.65, and 0.63 yr.

model are shown in Figs. 1c–e, respectively. The streamfunction exhibits a typical overturning circulation with a maximum value of about 10 Sv. This value is smaller than the estimated (15 ± 2) Sv (Ganachaud and Wunsch 2000) but consistent with other results obtained using this model in the absence of wind forcing (Stocker et al. 1994).

The linear tangent matrix **A** is calculated numerically using the full nonlinear model after it has been run to steady state for 12 000 yr as described in Huck and Vallis (2001). Perturbations of 0.0001°C and 0.0001 ppt are used in the prognostic equations. Huck and Vallis (2001) conclude that the eigenvalues and eigenmodes of the linear tangent matrix obtained in this way are rather insensitive to the amplitude of the perturbations. The eigenvalues of **A** all have negative real parts indicating a stable system: any initial perturbation to the system will decay to zero after a sufficiently long time, with a decay time scale for each mode given by the reciprocal of the real part of its eigenvalue. Modes with imaginary eigenvalues will oscillate as they decay with time scales of 2π times the reciprocal of the imaginary part of the eigenvalue. Figure 2a shows the decay and oscillatory time scales of the 800 modes of the system. The decay time scales range from days to thousands of years. Of the 800 modes, 552 oscillate as they decay with oscillation time scales ranging from decades to tens of thousands of years. The decay time scale appears to be independent of whether the mode oscillates, but the fastest decaying modes do not oscillate. This result is similar to that obtained from Zanna and Tziperman's (2005) coupled atmosphere–ocean model, in which it was also found that the very fast decaying modes did not oscillate.

As discussed in Tziperman and Ioannou (2002), a quantity representing the THC amplitude must be defined to study the growth of anomalies by the nonnormal linearized dynamics in the stable regime. This quantity $U(\phi)$ is analogous to the meridional overturning streamfunction defined in Eq. (12) and can be written in terms of the depth-averaged meridional velocity $v(\phi)$

$$U(\phi) = v(\phi)\Delta x H_{\text{top}}. \tag{18}$$

In the above, Δx is the width of the basin and

$$v(\phi) = \frac{1}{H_{\text{top}}} \int_{-H_{\text{top}}}^{0} v(\phi, z)dz, \tag{19}$$

where $H_{\text{top}} = 2000$ m. The meridional velocity is positive in the top 2000 m of the ocean and negative in the bottom 3000 m, thus the integration need only be over the top portion of the ocean. A plot of $U(\phi)$ as a function of latitude for the steady-state solution is shown in Fig. 1f. The maximum value occurs at about 72°N, which is consistent with the steady-state streamfunction reached by the full nonlinear model 12 000 yr after spinup (Fig. 1e).

The quantity to be maximized, $M(t = \tau)$, is the sum over latitudes of the squares of the THC anomaly amplitude,

$$M(t = \tau) = \sum_{\phi=0}^{90^o} |U(\phi, t = \tau)|^2 \tag{20}$$

(from this point onward, all state variables are perturbation quantities, so primes are dropped for notational convenience). Because the THC amplitude is proportional to the meridional velocity, $M(t = \tau)$ is a useful measure of the overall strength of the overturning circulation, which is quadratic in the state variables. Evaluating the THC anomaly at the single latitude (72°N) where $U(\phi)$ is a maximum rather than summing over all latitudes did not yield particularly interesting results: in this case, transient amplification and then decay did not occur. Instead, the THC anomaly was initially nonzero and simply decayed over time such that large anomalies occurred only at 72°N rather than over the whole domain. Zanna and Tziperman (2005) also found it dynamically uninteresting to use a norm kernel that maximized the transient growth of the THC at a single latitude.

In the linearized dynamics the THC amplitude is directly proportional to the state function according to $U(\phi, t) = R_\phi{}^{\mathrm{T}}\mathbf{P}(t)$, where R_ϕ is a linear operator relating temperature and salinity perturbations to overturning strength perturbation, corresponding to a discretized approximation to Eq. (18). The norm used to measure the growth of the state vector anomaly at time τ, $\mathbf{P}(\tau)$, follows from Eq. (20) with $M(\tau) = \mathbf{P}^{\mathrm{T}}(\tau)X\mathbf{P}(\tau)$, where the norm kernel matrix $\mathbf{X}$ is

$$\mathbf{X} = \sum_{\phi=0}^{90^o} (R_\phi R_\phi^{\mathrm{T}}). \tag{21}$$

A measure of perturbation growth or decay is the factor by which the norm changes over the time interval τ and is given by

$$\lambda = \frac{M(\tau)}{M(0)} = \frac{\mathbf{P}^{\mathrm{T}}{}_0\mathbf{B}^{\mathrm{T}}(\tau)\mathbf{X}\mathbf{B}(\tau)\mathbf{P}_0}{\mathbf{P}^{\mathrm{T}}{}_0\mathbf{X}\mathbf{P}_0}, \tag{22}$$

where $\mathbf{B}(\tau)$ is the propagator of the tangent linear equation, such that $\mathbf{P}(\tau) = \mathbf{B}(\tau)\mathbf{P}_0$. The optimal perturbation is that which yields the largest value of λ subject to the constraint that $M(0) = 1$. According to the Rayleigh–Ritz method, the optimal perturbation is the eigenmode of $\mathbf{B}^{\mathrm{T}}(\tau)\mathbf{X}\mathbf{B}(\tau)$ with the largest eigenvalue (Moore et al. 2003). The initial conditions $\mathbf{P}_0$ leading to an optimal growth at time τ are therefore the generalized eigenvectors of the generalized eigenvalue problem

$$\mathbf{B}(\tau)^{\mathrm{T}}\mathbf{X}\mathbf{B}(\tau)\mathbf{P}_0 = \lambda\mathbf{X}\mathbf{P}_0 \text{ subject to } \mathbf{P}_0{}^{\mathrm{T}}\mathbf{X}\mathbf{P}_0 = 1. \tag{23}$$

Because temperature and salinity perturbations can counteract each other so as to have no net effect on the strength of the overturning, Eq. (21) results in a singular matrix (i.e., its determinant is zero), which in turn may result in infinite amplification factors over finite time. In an unpublished study of transient growth done by J. Alexander for the THC in Griffies and Tziperman's (1995) four-box model, the singular norm kernel defined in Eq. (21) leads to two of the eight eigenmodes having infinite amplification. This nonuniqueness of the optimal eigenmodes may result in a suboptimal transient growth estimate (Tziperman and Ioannou 2002). To eliminate this possibility, Tziperman and Ioannou (2002) regularize the norm kernel by adding a small diagonal matrix to $\mathbf{X}$ to create a nonsingular matrix. In this study, a matrix with diagonals less than 0.005% of the maximum element of $\mathbf{X}$ was added to $\mathbf{X}$, resulting in a matrix with small but nonzero determinant.

The time scale for optimal growth τ_{opt} is the value of τ maximizing the amplification factor λ; a plot of λ as a function of τ is given in Fig. 3. Following the same logic as Sevellec et al. (2007), the first peak that occurs at $\tau =$ 0.4 yr is disregarded because this time scale is too small to be relevant in our 2D model. The second maximum where $\tau_{\text{opt}} = 6$ yr was the time scale used in the propagator matrix for all subsequent calculations. It should be noted here that for nonnormal systems, amplification processes are the result of the combination of two effects: one that is normal with a time scale governed by the least damped eigenmode and one that is nonnormal with a time scale representing transient growth (Trefethen 1997). Thus, the time scales of the individual eigenmodes of the system are not necessarily the same as the time scale of the transient amplification of perturbations.

The optimal initial salinity and temperature perturbations calculated from the linearized model equations that maximize the transient amplification of the THC anomaly for $\tau = 6$ yr are shown in Figs. 4a,b. The evolution of these anomalies is shown in Figs. 4c–h. The temperature and salinity optimal initial conditions have

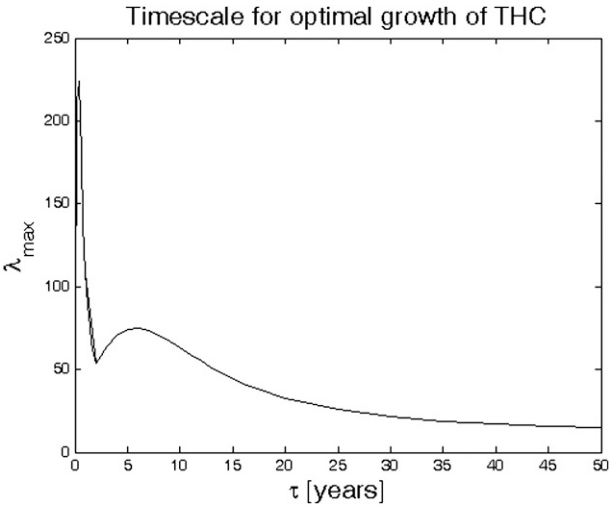

FIG. 3. Maximum amplification factor [Eq. (22)] of the linearized model as a function of time.

a dipole structure between 70° and 80°N with negative temperature and positive salinity anomalies on the surface and with anomalies of opposite sign at depth. At $t = 6$ yr (Figs. 4e,f), the time of maximum amplification, the sign of the anomalies in the dipole have reversed for the temperature but not for the salinity. In both cases the anomalies have spread over a wider depth range. As the anomalies decay, they continue to spread out over an even wider range of space. Because temperature and salinity anomalies significantly redistribute in space as they amplify, rather than simply undergo localized growth, this implies that both advection and nonlocalized effects contribute to the transient growth. The slow decay of the temperature and salinity anomalies is governed by horizontal and vertical diffusion.

The evolution of the THC anomaly, $U(\phi, t) = R_\phi \mathbf{P_0}(t)$, and the contributions to the THC anomaly from the thermally and salinity-driven components are displayed as a function of latitude in Figs. 5a–f. Initially, the thermally and salinity-driven components tend to cancel each other so that the THC anomaly is nearly zero at $t = 0$ (Fig. 5a). This is consistent with previous studies of THC transient amplification using both box models (Zanna and Tziiperman 2008; Tziperman and Ioannou 2002) and GCMs (Tziperman et al. 2008). The different evolutions of the temperature and salinity anomalies lead to growth at later times with the salinity contribution dominating the overall amplification of the THC. The maximum growth of the THC occurs at 76.5°N at $t = 6$ yr (Fig. 5d). Throughout most of the evolution of the perturbation, anomalies in each of the temperature and salinity contributions to the THC are of opposite signs and are concentrated in the middle and high latitudes. After 50 yr, the salinity and temperature components once again exactly cancel one another and the THC amplitude falls to zero (Fig. 5f). Note that strong anomalies in both temperature and salinity persist for many decades after the anomaly in overturning strength has decayed.

Figures 6a–d show the time evolution of the linear THC amplitude and the contributing salinity and temperature components for latitudes 18°, 36°, 54°, and 76.5°N, respectively. In these plots it can be seen again that the contributions from both the thermally and salinity-driven components are significant with the salinity dominating at 76.5°N where the growth of the THC is a maximum (Fig. 6d). At the lower latitudes the salinity component initially dominates the growth, but after the first 6 yr when the maximum amplification has been reached and the anomalies begin to decay, the thermally driven component dominates the decay. The decay time for the components is longer at low latitudes than it is at high latitudes (Figs. 6 a–c). Note that at some latitudes the intensification of the overturning strength locally is preceded by a slight weakening.

The THC salinity and temperature components as a function of time and latitude are shown in Figs. 7a,b. Because the contributions from the salinity and temperature components are of opposite sign, the negative of the temperature contribution is plotted, enabling an easier comparison of their magnitudes and time scales. It can be seen that the salinity contribution reaches a larger maximum value than the temperature contribution, while the spatial structures are very similar. The dominance of the salinity contribution to the total THC can be seen by noting that the sign of the total THC amplitude is the same as the sign of the salinity component (cf. Fig. 8b, 7a).The growth of the thermally and salinity-driven components of the THC tends to occur for longer periods than the growth of the total THC (Fig. 8b), because the two contributing components tend to cancel each other after about 50 yr.

For the above analyses it has been assumed that the evolution of the THC anomaly is governed by linear dynamics. It is therefore important to compare the evolution of the THC anomaly amplitude $U(\phi)$ calculated using the full nonlinear model to that calculated using the linear model. This was done by adding the optimal initial conditions state vector (of small norm) to the steady-state solution of the WS model and then running the full nonlinear model for a further 200 yr. The THC anomaly amplitude calculated from the nonlinear model exhibits a similar transient growth pattern as that of the linear model (Fig. 8a). The differences are small enough that we may conclude that the linear approximation is valid for sufficiently small perturbations.

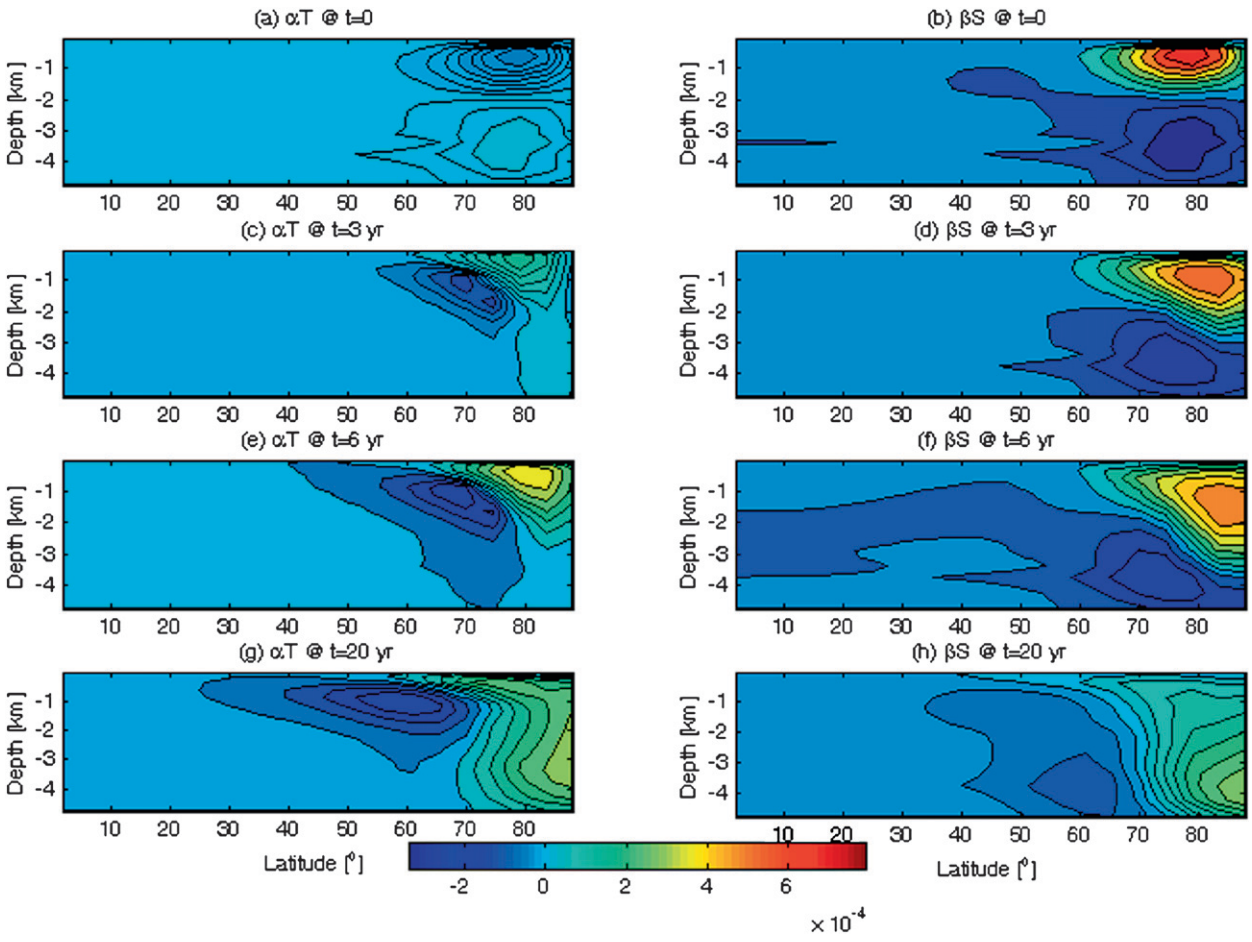

FIG. 4. (a) Optimal initial temperature perturbation (αT) and (b) optimal initial salinity perturbation (βS) calculated from the linearized model equations that maximize the transient amplification of the THC for $\tau = 6$ yr. (c)–(h) The αT and βS perturbations at 3, 6, and 20 yr.

b. *Dynamically relevant eigenmodes*

Even though all of the eigenmodes of the linear operator $\mathbf{A}$ are stable, the nonnormality of $\mathbf{A}$ results in nonorthogonal, linearly dependent eigenmodes. Transient perturbation growth results from the linear interference of nonorthogonal eigenmodes with different decay times. The time scale of the transient amplification is typically the same as the time scale of the fastest decaying relevant eigenmode (Farrell and Ioannou 1996). The decay of the perturbations is then governed by the slowest decaying relevant eigenmode. The amount of perturbation growth possible is proportional to the degree of linear dependence of the eigenmodes (Aiken et al. 2002). To investigate the ''optimal'' eigenmodes of the linear operator, which participate in the observed perturbation growth, the optimal initial conditions $\mathbf{P}_0$ are projected onto the eigenmodes of $\mathbf{A}$ (Farrell and Ioannou 1996).

The eigenvalue spectra of $\mathbf{A}$ and $\mathbf{A}^{\mathrm{T}}$ are identical, each having eigenvalues that occur in complex conjugate pairs. Let $\{\lambda_n, \hat{s}_n\}$ and $\{\sigma_n, \hat{r}_n\}$ be the {eigenvalue, eigenvector} sets of $\mathbf{A}$ and $\mathbf{A}^{\mathrm{T}}$, respectively, where $\lambda_n^* = \sigma_n$ and * denotes complex conjugate. The biorthogonality property between the eigenmodes of $\mathbf{A}$ and $\mathbf{A}^{\mathrm{T}}$ can be stated as

$$\hat{s}_n^{\mathrm{T}} \hat{r}_m (\lambda_n - \sigma_m^*) = \hat{s}_n^{\mathrm{T}} \hat{r}_m (\lambda_n - \lambda_m) = 0, \tag{24}$$

so $\lambda_n = \lambda_m$ for $n = m$ and $\hat{s}_n^{\mathrm{T}} \hat{r}_m = 0$ for $n \neq m$. The state vector $\mathbf{P}_0$ can be written as a linear superposition of the eigenmodes with projection coefficients a_k:

$$\mathbf{P}_0 = \sum_{k=1}^{k=800} a_k \hat{s}_k. \tag{25}$$

Because the perturbation has unit norm, $\mathbf{P}_0{}^{\mathrm{T}} \mathbf{X} \mathbf{P}_0 = 1$, the amplitude of the kth eigenmode is

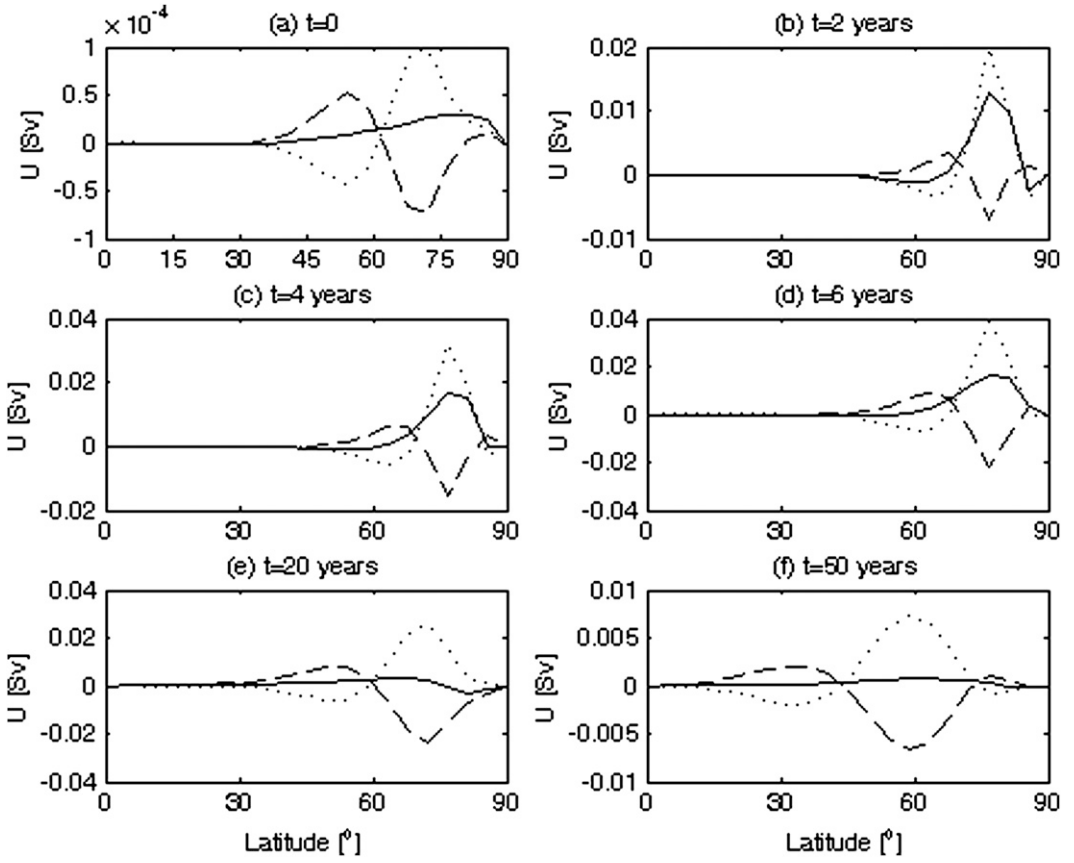

FIG. 5. Evolution of the linear THC anomaly (solid line) and the contributions from the temperature (dashed line) and salinity (dotted line) as a function of latitude calculated from the linearized model equations starting from the optimal initial conditions that maximize the transient amplification of the THC anomaly for $\tau = 6$ yr. (a) $t = 0$, (b) $t = 2$ yr, (c) $t = 4$ yr, (d) $t = 6$ yr, (e) $t = 20$ yr and (f) $t = 50$ yr. (Note that the scaling of each plot is different and the maximum amplification occurs at $t = 6$ yr.)

$$a_k = \hat{r}_k{}^{\mathrm{T}}\mathbf{P}_0/\hat{r}_k{}^{\mathrm{T}}\hat{s}_k. \tag{26}$$

To determine which eigenmodes are responsible for the transient amplification of the THC, the projection coefficients for each eigenvector of the generalized eigenvalue problem $\mathbf{B}(\tau)^{\mathrm{T}}\mathbf{X}\mathbf{B}(\tau)\mathbf{P} = \lambda\mathbf{X}\mathbf{P}$ are calculated using Eq. (26). Each of these 800 eigenvectors has a corresponding a_i series of 800 values corresponding to the 800 eigenmodes of the system. These sets of projection coefficients are plotted in Fig. 9a. The eigenmodes denoted by k are arranged according to increasing modulus of the eigenvalues of $\mathbf{A}$. The eigenmodes that consistently have large projection coefficients are the ones that are favored by the optimal vectors. These eigenvectors are also among the ones favored by the optimal initial conditions. The projection coefficients for the optimal initial conditions are many orders of magnitude smaller than the largest projection coefficients, but when choosing the preferred eigenmodes, we are interested in their relative magnitudes for each given eigenvector rather than their absolute magnitudes. It can be seen in Fig. 9b that five modes have consistently large projection coefficients. Two are oscillating complex conjugate pairs (641,642) with decay and oscillation time scales of 0.72 and 1420 yr, respectively, and (667,668) with decay and oscillation time scales of 0.63 and 478 yr, respectively. The other three favored eigenmodes are purely decaying ones (658,659, 666) with decay times of 0.65, 0.65, and 0.63 yr, respectively.

The contribution of an eigenvector to the nonnormality of $\mathbf{A}$ can be quantified by the factor $\nu(k) = |\hat{s}_k||\hat{r}_k|/(\hat{r}_k{}^{\mathrm{T}}\hat{s}_k)$ (Farrell and Ioannou 1993a), where $\hat{r}_k$ is the biorthogonal of $\hat{S}_k$ (the eigenvector that is orthogonal to all other eigenvectors). For real eigenvectors, $\nu(k)$, is the secant of the angle between the eigenvector and its biorthogonal. A plot of $|\nu(k)|$ versus $|a(k)|$ for the optimal initial condition $\mathbf{P}_0$ is shown in Fig. 10a. The five eigenmodes (circled in blue) that have consistently large projection coefficients at $t = 0$ are also the most

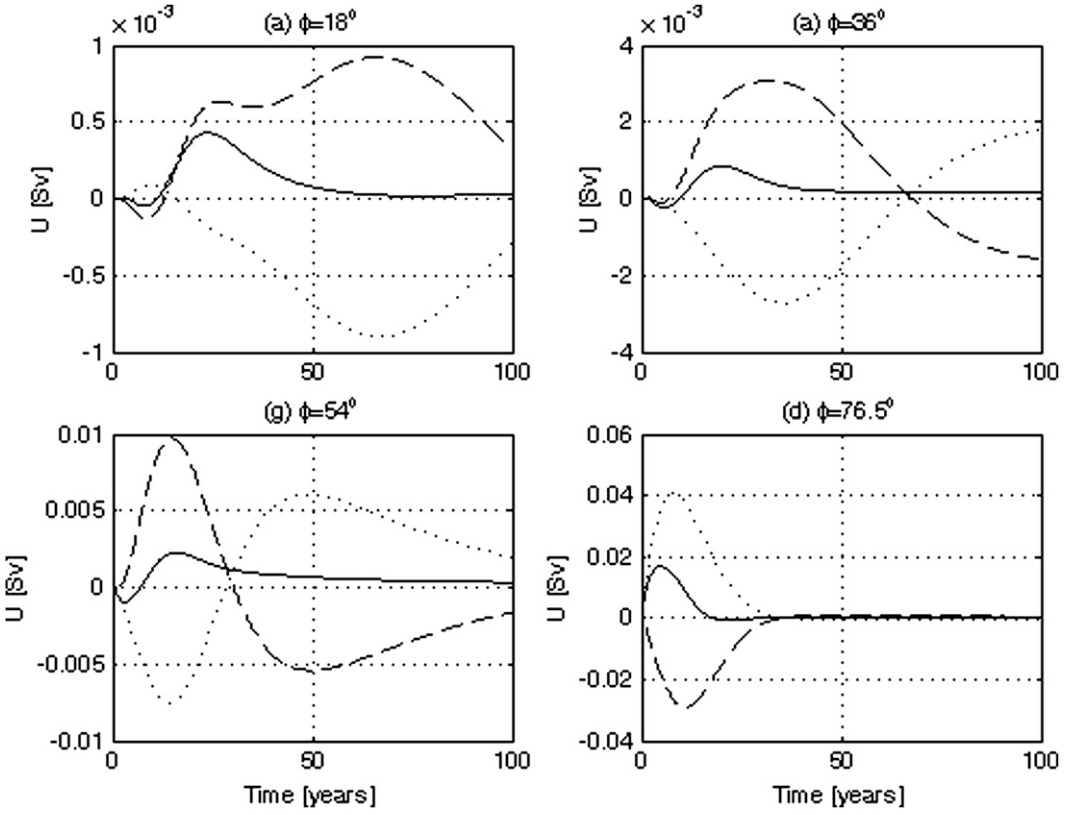

FIG. 6. Evolution of the linear THC anomaly (solid line) and its contributions from the temperature (dashed line) and salinity (dotted line) as a function of time calculated from the linearized model equations starting from the optimal initial conditions that maximize the transient amplification of the THC anomaly for $\tau = 6$ yr. (a) $\varphi = 18°$, (b) $\varphi = 36°$, (c) $\varphi = 54°$, and (d) $\varphi = 76.5°$. (Note that the scaling of each plot is different and the maximum amplification occurs at 76.5°.)

highly nonnormal eigenvectors. However, these five eigenmodes alone are not sufficient for producing transient amplification of THC anomalies. Although the degree of nonnormality does not change as the system evolves in time, the projection coefficients do change as the state vector $\mathbf{P}(t)$ evolves. To gain further insight into the eigenmodes that are responsible for the transient amplification of THC anomalies on a time scale of 6 yr, the state vector at $t = 6$ yr was projected onto the eigenmodes of $\mathbf{A}$. Figure 10b shows a plot of $|\nu(k)|$ versus $|a(k)|$ at $t = 6$ yr. It can be seen that the five highly nonnormal modes (circled in blue) no longer have large projection coefficients at $t = 6$ yr, indicating that their contribution to the transient amplification is only important close to $t = 0$. This is consistent with nonnormal operators whose transient behavior differs entirely from the asymptotic behavior suggested by the eigenvalues. The eigenmodes that contribute most to the maximum amplification of the THC anomalies at $t = 6$ yr are the ones with large projection coefficients in Fig. 10b (circled in red in both Figs. 10a,b). Eleven pairs of oscillating eigenmodes with decay time scales ranging from 2 to 6 yr and oscillation time scales ranging from 35 to 95 yr were found to be the most significant contributors to the amplification process. The decay and oscillation time scales of these 11 pairs of modes as well as the 2 oscillating highly nonnormal modes are shown in Fig. 2b. The eigenmodes with relatively large projection coefficients that are not circled in Fig. 10b all have decay time scales less than 2 yr. When these modes were added to the initial perturbation, the amplification shown in Fig. 11 did not change significantly; these modes do not appear to play an important role in the transient amplification process.

Combining the five highly nonnormal eigenmodes that are important to the amplification process during the initial few years with the 11 oscillating pairs of modes that are important at the time of maximum amplification leads to a fairly good representation of the transient amplification of the THC. Figure 11 shows the evolution of the linear THC anomaly produced by these 13 pairs of oscillating eigenmodes and three

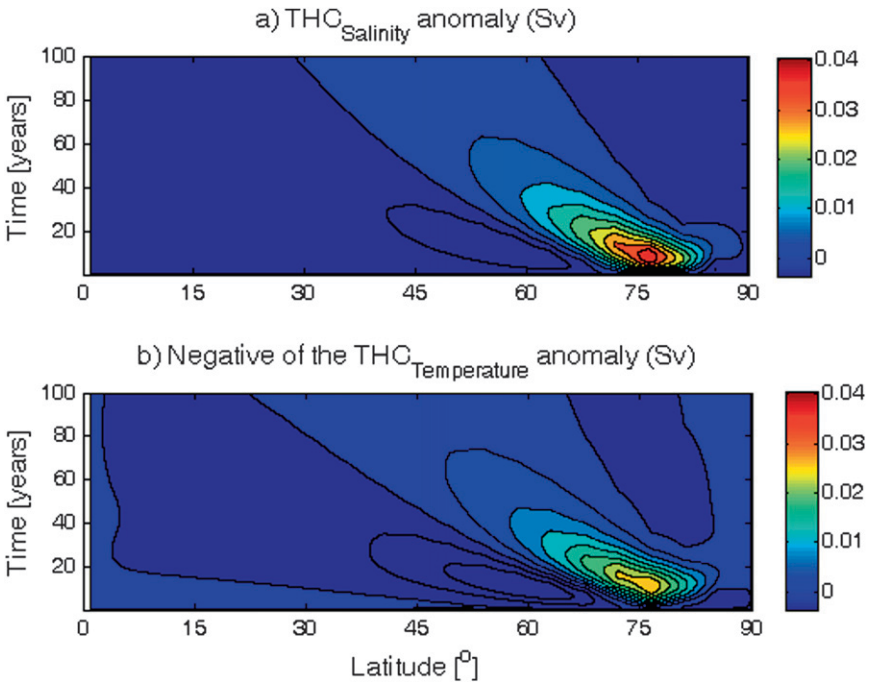

FIG. 7. Evolution of the (a) salinity component of the THC amplitude and (b) negative of the temperature component of the THC amplitude as a function of time and latitude calculated from the linearized model equations starting from the optimal initial conditions that maximize the transient amplification of the THC anomaly for $\tau = 6$ yr.

nonoscillating eigenmodes and by the full set of 800 eigenmodes at 76°N (the latitude where maximum amplification occurs). Note that the amplification is in fact greater for the full system than for the low-dimensional projection because the initial perturbation is much smaller. The evolution of a typical optimal perturbation in a nonnormal system is determined by the evolution of the interference pattern of the relevant eigenmodes rather than by the growth or decay of individual eigenfunctions. The fact that the important eigenmodes shown to be responsible for the transient amplification of THC anomalies in this study have very small decay time scales (less than 10 yr) when compared to the time scale of the amplification process is evidence of the importance of the interference process when considering the response of this system to perturbations.

5. Discussion

a. Sensitivity studies

The overturning strength in the WS model is strongly affected by the value of the vertical diffusivity K_v (Wright and Stocker 1992), a quantity that is not well constrained by observations. To investigate the role that vertical diffusivity plays in the nonnormal dynamics of transient THC amplification, the analysis was repeated for a range of vertical diffusivities (see Table 1). We found that by increasing the vertical diffusivity from $K_V = 0.2 \times 10^{-4}\,\mathrm{m^2\ s^{-1}}$ to $K_V = 1.0 \times 10^{-4}\,\mathrm{m^2\ s^{-1}}$ in the absence of wind forcing, the value of the maximum streamfunction increased from 4.3 to 9.7 Sv (1 Sv $\equiv 10^6\ \mathrm{m^3\ s^{-1}}$). Wright and Stocker (1992) obtained a similar result in the absence of wind forcing. Although the strength of the streamfunction from the WS model used in this study has been shown to be sensitive to variations in K_V, our analyses show that the nonnormal dynamics that lead to transient amplification of the THC is not highly sensitive to variations in K_V.

The optimal initial conditions over the range of vertical diffusivities used here do not differ significantly in either strength or spatial pattern, while the value of the maximum amplification of the THC anomaly from Eq. (22) increases from 22 to 75. Furthermore, the general patterns of growth and decay of the two contributions to the THC anomaly amplitude are not affected by changing the vertical diffusivity. Both the dominance of the salinity component in the THC anomaly growth and the latitude of maximum growth are also independent of vertical diffusivity.

The quantity that does depend strongly on vertical diffusivity in the nonnormal analysis of the THC growth

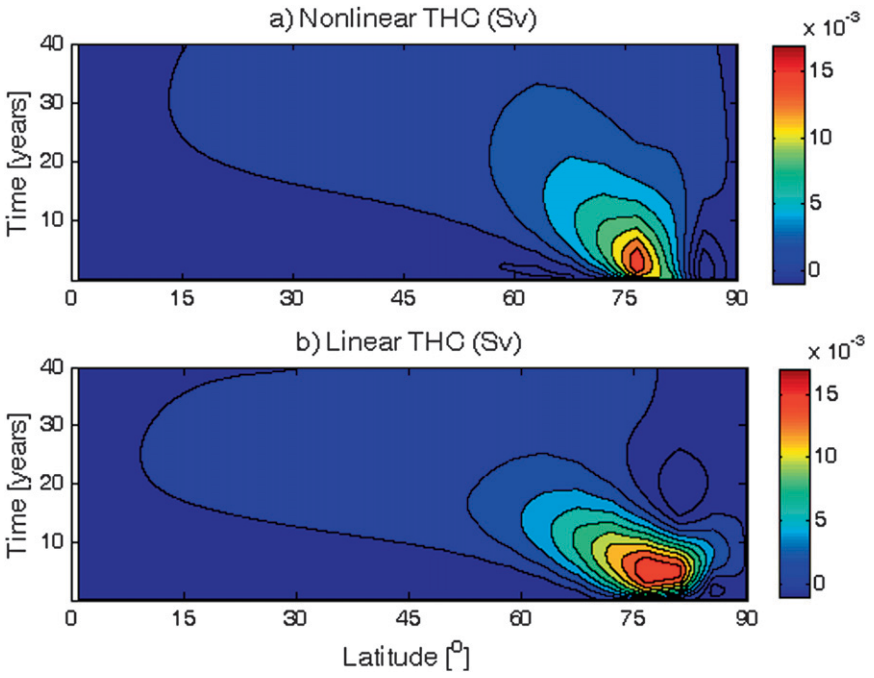

FIG. 8. (a) THC anomaly calculated from the full nonlinear model and (b) THC anomaly calculated from the linearized model equations starting from the optimal initial conditions that maximize the transient amplification of the THC anomaly for $\tau = 6$ yr.

is the time of maximum amplification. It was found that increasing K_V by a factor of 5 (while keeping all other variables constant) decreased the optimization time by about a factor of 3 (almost the same factor as for amplification). Note that increasing K_V increases the mean overturning strength, so a reduction in the amplification time scale is consistent with an increase in the rate of anomaly advection (although this does not account entirely for the reduction in the amplification time scale). The optimization time was also found to be dependent on the relaxation time scales of the temperature and salinity boundary conditions. Changing the relaxation time scales from 50 days for each of the temperature and salinity to 30 days for the temperature time scale and 120 days for the salinity time scale (while keeping the vertical diffusivity fixed at $K_V = 0.2 \times 10^{-4}\,\mathrm{m^2\ s^{-1}}$) resulted in the optimization time changing from 25 to 19 yr. Once again, the mechanism of transient amplification of the THC was not affected by this change, even though the value of the maximum amplification decreased from 55 to 22.

b. *Amplification time scale*

In general, 2D zonally averaged models are not expected to permit the investigation of some ocean processes characterized by time scales less than a decade and by horizontal spatial scales less then several hundred to thousand kilometers. The two main processes that drive the meridional overturning circulation are the traditional thermohaline mechanism that results in mixing of heat from the surface to the deep water and the wind-driven upwelling caused by the strong westerly circumpolar winds in the Southern Ocean. The time scales associated with these processes are much longer than a decade, but these processes do not fully determine the Atlantic meridional overturning circulation's spatial extent and strength (Kuhlbrodt et al. 2007). Horizontal gyre circulation, atmospheric cooling, precipitation, evaporation, and ice melting are some of the variety of processes that can affect the strength and spatial pattern of the meridional overturning circulation. The time scales for these localized processes are usually less than a decade. Even when a model does not explicitly resolve these processes, studies have shown that ocean processes characterized by time scales less than a decade can be investigated using 2D zonally averaged models.

Hirschi and Stocker (2002) found that a 3D ocean general circulation model and the WS 2D zonally averaged ocean model produced similar patterns and time scales of propagation of density anomalies. They applied freshwater perturbations at 47.5°S for 2 months and studied the propagation of the resulting density anomalies. The 3D ocean model showed a sharp density

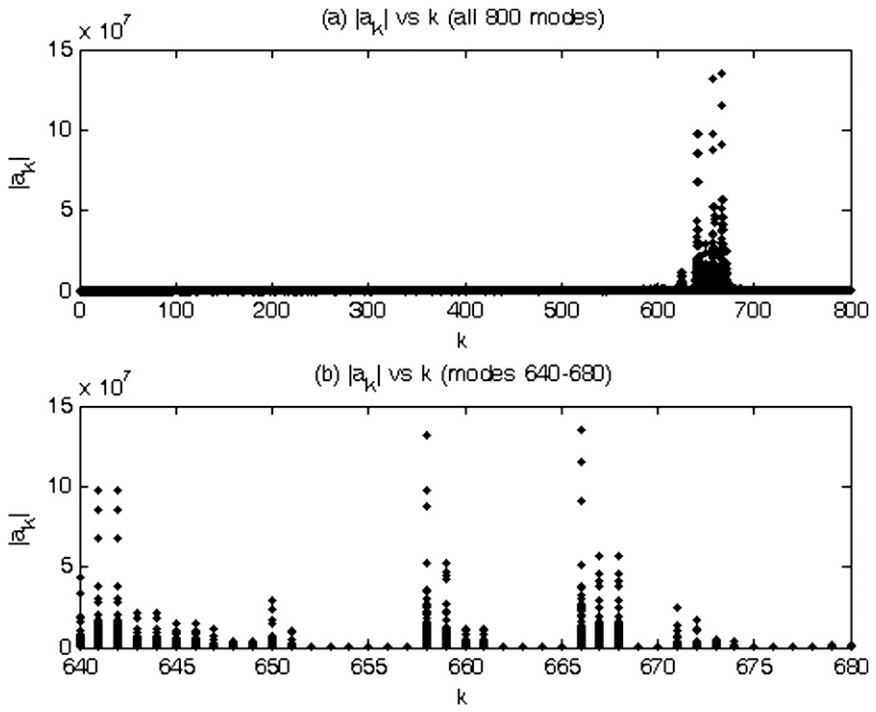

FIG. 9. (a) Projection coefficients computed by projecting each eigenvector of Eq. (23) onto the full set of 800 eigenmodes ($k = 1,\ldots,800$). The amplitude coefficients for all 800 eigenvectors are shown for each k and (b) projection coefficients for eigenmodes ($k = 640,\ldots,680$).

signal that propagated as an internal oceanic Kelvin wave reaching the midlatitudes of the Northern Hemisphere within 2 yr. In the zonally averaged model, the density signal reached the midlatitudes of the Northern Hemisphere after about 5–10 yr. Although the 2D model responded more slowly to the perturbation than did the 3D model, this study showed that the density anomalies in the zonally averaged model propagated faster than color tracers being carried by advection/diffusion. This study also found that the time tendency of the maximum northern meridional overturning cell reached a maximum value after 7–8 yr in the 2D zonally averaged model, indicating that subdecadal processes can be captured in such a model. Other studies using the WS 2D zonally averaged model have also investigated processes with time scales less than a decade. Schmittner and Stocker (2001) found that the WS model was able to simulate a global overturning that exhibited a strong seasonal cycle in agreement with 3D ocean models. They found that rapid changes in the maximum streamfunction in the Atlantic occurred on a seasonal time scale when fast freshwater flux perturbations were applied to the model.

In this study we are interested in the transient amplification of the THC due to the nonnormal nature of the tangent linear operator. Because we found that this mechanism is not strongly dependent on the values of vertical diffusivity or relaxation time scales of the surface temperature and salinity fields, we have chosen the region of parameter space that gives the most realistic value for the maximum streamfunction, 10 Sv, in the absence of wind forcing ($K_V = 1.0 \times 10^{-4}\,\mathrm{m^2\,s^{-1}}$, $\Gamma_T = 30$ days, and $\Gamma_S = 120$ days). Although this gives a time scale for amplification that is only 6 yr, this value agrees with the time scales for growth found in two other similar studies of nonnormal transient amplification of the THC. Using a coupled ocean–atmosphere GCM, Tziperman et al. (2008) found the amplification time scale to be between 5 and 10 yr, while Zanna and Tziperman (2008) calculate the time scale for maximum amplification of the THC to be 9 yr in their 2D zonally averaged coupled ocean–atmosphere box model. Another supporting result from the GCM study is that the growth of temperature and salinity anomalies occurred largely in the meridional direction, indicating that the 2D model may be adequate for capturing the complex linearized dynamics of nonnormal THC perturbation growth.

c. Comparison to previous studies

Although the present study is the first to consider optimal perturbation growth of the THC involving both temperature and salinity fields using the WS model,

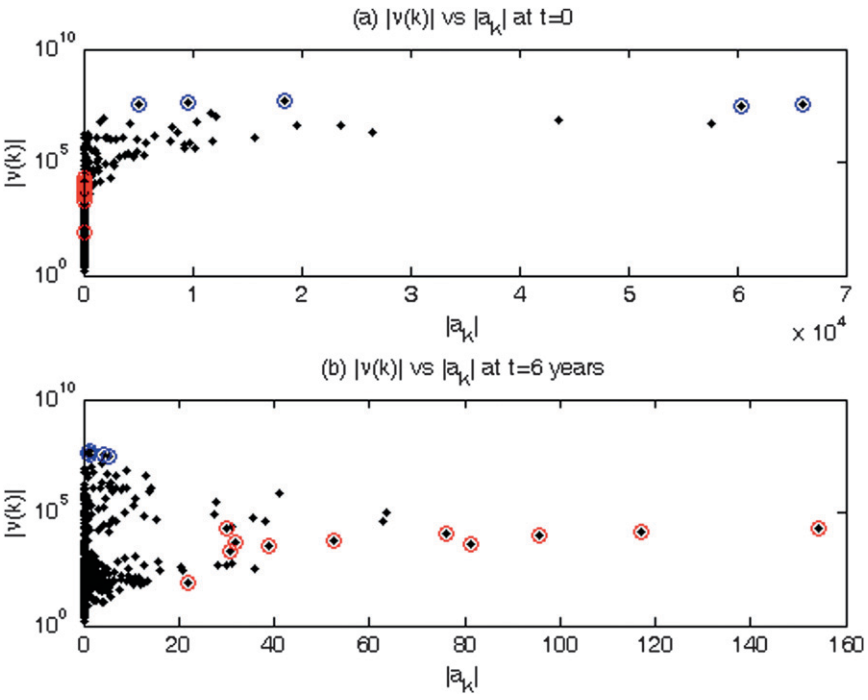

FIG. 10. (a) $|v(k)|$ vs $|a_k|$ for $k = 1, \ldots, 800$ for $\mathbf{P}_0$, the optimal initial conditions and (b) $|v(k)|$ vs $|a_k|$ for $k = 1, \ldots, 800$ for $\mathbf{P}_6$, the state vector at $t = 6$ yr. The 13 pairs of oscillating modes and 3 nonoscillating modes responsible for the transient amplification are circled in (a) and (b).

previous studies have considered transient growth. The first study to apply the ideas of nonnormal dynamics to the THC was that of Lohmann and Schneider (1999), in which the nonnormal properties of the Stommel two-box model of the THC were considered. They found that the optimal perturbation affecting long-term climate variability had little resemblance to the most unstable mode of the system. Their results suggested that climatic states associated with North Atlantic Deep Water (NADW) formation were located in a specific part of the phase space only where the NADW circulation with a large meridional salinity or small temperature gradient was not stable. This is supported by Tziperman (1997), who found inherently unstable climate behavior due to a weak THC. In agreement with the results of Lohmann and Schneider (1999), the present study finds that nonnormal dynamics lead to perturbations involving both temperature and salinity, which display pronounced transient growth. The amplification time scale found in Lohmann and Schneider (1999) was shorter than that found in the present study, but detailed quantitative agreement cannot be expected because of the highly idealized nature of the model used in the earlier study.

Tziperman and Ioannou (2002) presented a detailed analysis of nonnormal dynamics of the THC using a three-box model, for which two physical mechanisms for the transient amplification of the THC were identified. One, with a transient amplification time scale of approximately 2 yr, involved an interaction between the THC anomaly induced by rapidly decaying sea surface

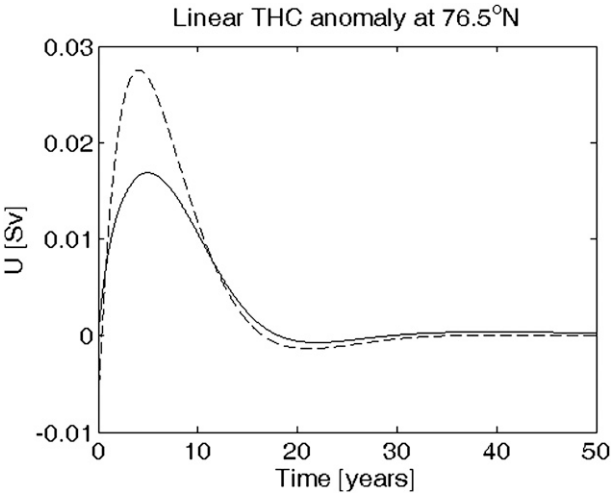

FIG. 11. Evolution of the linear THC anomaly from all 800 eigenmodes (solid line) and from the top 13 pairs of oscillating eigenmodes and three nonoscillating eigenmodes (dotted line).

TABLE 1. The maximum value of the streamfunction, time scale for optimum growth, and maximum amplification of the THC anomaly for different vertical diffusivities and relaxation times for the surface salinity and temperature.

Vertical diffusivity ($m^2\ s^{-1}$)	Salinity relaxation time (days)	Temperature relaxation time (days)	Max streamfunction (Sv)	Optimization time (yr)	Max amplification
0.2×10^{-4}	50	50	4	25	55
0.2×10^{-4}	120	30	4	19	22
0.4×10^{-4}	120	30	6	11	43
0.6×10^{-4}	120	30	7	8	60
0.8×10^{-4}	120	30	8	7	69
1.0×10^{-4}	120	30	10	6	75

temperature anomalies and the THC anomaly induced by the slower decaying salinity modes. The second mechanism of transient amplification was primarily driven by an interaction between different slowly decaying salinity modes, and it had a typical growth time scale of few decades. For both mechanisms, the initial THC anomaly was zero because of the offsetting effects of temperature and salinity anomalies on the meridional density gradient. This earlier study agrees with the present study in finding substantial transient amplification on decadal time scales that is dominated by salinity dynamics and involves both temperature and salinity.

Transient amplification of the THC in a less idealized model was studied by Zanna and Tziperman (2005), who employed a two-dimensional coupled box atmosphere–ocean model to investigate possible physical mechanisms for the transient growth of THC anomalies. This study found transient growth displaying maximum amplification after 42 yr with optimal perturbations involving both temperature and salinity anomalies. This more recent study found that the amplification mechanism was the result of an interaction between a few damped (oscillatory and nonoscillatory) modes with decay times between 20 and 800 yr. In agreement with this earlier study, the present study finds that the optimal perturbation leading to the greatest transient growth involves interactions between temperature and salinity anomalies, which combine in the initial conditions to produce a negligible initial THC perturbation. The present study finds that the amplification mechanism is the result of an interaction between 5 highly damped and 11 oscillatory eigenmodes and their complex conjugates with oscillation times between 35 and 95 yr. Both the previous study and the present study find that it is impossible to produce an initial THC perturbation of zero when using only the small subset of all dynamical modes that dominate the transient growth of the THC. All of the eigenmodes of the system are required to produce an initial perturbation of zero.

In a recent study, Sevellec et al. (2007) use a 2D latitude–depth ocean thermohaline circulation model to study the variability of the ocean circulation perturbed by a freshwater flux and also find that the nonnormality of the dynamics leads to transient growth of the overturning circulation intensity. However, in the study of Sevellec et al. (2007), only surface salinity optimal perturbations are used to excite the THC: the temperature component is not included. This study finds that the maximum response of the circulation intensity occurred after 67 yr, associated with a single weakly damped linear eigenmode with an oscillation time scale of 150 yr. In the present study, with both active temperature and salinity contributions to the density of seawater, the time scales of optimal THC amplification and decay are considerably shorter. Perturbations in temperature and salinity persist for many decades, but in such a way that they counterbalance to produce little effect on the overturning strength after about 50 yr. Sevellec et al. (2007) also obtain very different results from truncating the contributions from the eigenmodes of the linear operator, concluding that only a couple of eigenmodes and their biorthogonals determine the effect of initial perturbations on long time scales and that the finite growth for the overturning intensity is due to a single oscillatory mode. We also find that the finite growth is dominated by a small number of eigenmodes. The initial cancellation of the salinity and temperature contributions to the THC anomaly is governed by the most highly nonnormal eigenmodes, and the subsequent evolution of this cancellation is governed by 11 pairs of oscillating eigenmodes.

Using the Geophysical Fluid Dynamics Laboratory (GFDL) coupled atmosphere–ocean general circulation model CM2.1, Tziperman et al. (2008) investigated the transient amplification of temperature, salinity, and THC anomalies due to nonnormal dynamics; they found that there was significant growth of all anomalies with a typical growth time of 5 to 10 yr with the THC anomaly displaying its maximum value at $t = 6$ yr. Many sensitivity studies were done to test the robustness of this time scale, and it was found that while the time scale was robust to parameter changes in their linearized model,

the actual value of the amplification was not. The main conclusion drawn from this inverse modeling study was that the nonnormality of the THC dynamics cannot be ignored when estimating reliable predictability limits. The structure of the initial condition of the ocean–atmosphere state will influence the amplification of the THC after a length of time smaller than the expected decadal or centennial variability time scale of the THC.

6. Conclusions

Characterizing the variability of the thermohaline circulation is important for understanding internal variability in the earth's climate system and for detecting trends of anthropogenic origin. In this study, we have applied the ideas of generalized linear stability theory to the dynamics of the thermohaline circulation described by a 2D zonally averaged ocean model. As a result of nonnormality of the linarized dynamics, nonorthogonal eigenmodes with different decay times interfere to create transient growth of THC anomalies in an asymptotically stable system. We examined the optimal initial conditions that lead to this transient growth using the tangent linear equation linearized about the steady state and found that the maximum amplification of the THC anomaly occurs after about 6 yr.

The major conclusions to be drawn from this study are the following:

- it is possible to obtain significant transient amplification of the THC;
- the amplification process involves temperature and salinity anomalies that combine to create a THC anomaly that is initially close to zero;
- the transient growth of the THC is dominated by the salinity dynamics;
- large temperature and salinity anomalies persist long after the overturning strength anomaly has decayed;
- many latitudes show an initial decrease in THC strength before the intensification occurs;
- it is possible to identify a small subset of the dynamics that are responsible for the amplification process (the most nonnormal modes account for the cancellation of the salinity and temperature components of the THC anomalies at $t = 0$); and
- the mechanism of amplification is insensitive to model parameters, while the timing of the amplification is sensitive.

The dynamics considered in this study were of pure thermohaline circulation, as wind forcing was not accounted for. In reality, the meridional overturning circulation is strongly affected by surface wind forcing; a natural extension of the present study is to consider optimal perturbation growth in the presence of surface winds. Furthermore, only a single hemisphere and ocean basin were considered in this study; a natural extension would consider the entire Atlantic basin.

Another important direction of research is the determination of the relevance of the optimal perturbations to the response to fluctuating surface forcing. The initial perturbation resulting in optimal transient amplification of the overturning circulation identified in this study is dominated by high-latitude surface anomalies of salinity and temperature and also involves anomalies at depth. Fluctuations in surface forcing can be expected to project on these optimal perturbations, but not perfectly. The relevance of these optimal perturbations to forced variability of the THC is characterized by the strength of the projection of the stochastic optimals (the spatial structures of the noise that result in maximum variance of the THC) on the optimal perturbations, the analysis of which is the goal of a future study. This research will provide insight into how the optimal perturbations characterized in this study may be realized physically and of the role they play in the variability of the THC.

Acknowledgments. The authors thank Laure Zanna for her helpful advice on this research. Julie Alexander would like to acknowledge support from the Canadian Foundation for Climate and Atmospheric Sciences. Adam Monahan would like to acknowledge support from the Natural Sciences and Engineering Research Council of Canada, the Canadian Foundation for Climate and Atmospheric Sciences, and the Canadian Institute for Advanced Research Earth System Evolution Program. The authors thank Thomas Stocker for sharing the source code for the WS model.

REFERENCES

Aeberhardt, M., M. Blatter, and T. F. Stocker, 2000: Variability on the century time scale and regime changes in a stochastically forced zonally averaged ocean-atmosphere model. *Geophys. Res. Lett.,* **27,** 1303–1306.

Aiken, C. M., A. M. Moore, and J. H. Middleton, 2002: The nonnormality of coastal ocean flows around obstacles, and their response to stochastic forcing. *J. Phys. Oceanogr.,* **32,** 2955–2974.

Clark, P. U., N. G. Pisias, and T. F. Stocker, 2002: The role of the thermohaline circulation in abrupt climate change. *Nature,* **415,** 863–869.

DelSole, T., and B. F. Farrell, 1995: A stochastically excited linear system as a model for quasigeostrophic turbulence: Analytic results for one- and two-layer fluids. *J. Atmos. Sci.,* **52,** 2531–2547.

Farrell, B. F., and P. J. Ioannou, 1993a: Stochastic dynamics of baroclinic waves. *J. Atmos. Sci.,* **50,** 4044–4057.

——, and ——, 1993b: Stochastic forcing of perturbation variance in unbounded shear and deformation flows. *J. Atmos. Sci.,* **50,** 200–211.

——, and ——, 1995: Stochastic dynamics of the midlatitude atmospheric jet. *J. Atmos. Sci.,* **52,** 1642–1656.

——, and ——, 1996: Generalized stability theory. Part I: Autonomous operators. *J. Atmos. Sci.,* **53,** 2025–2040.

Ganachaud, A., and C. Wunsch, 2000: Improved estimates of global ocean circulation, heat transport and mixing from hydrographic data. *Nature,* **408,** 453–457.

Griffies, S. M., and E. Tziperman, 1995: A linear thermohaline oscillator driven by stochastic atmospheric forcing. *J. Climate,* **8,** 2440–2453.

Hirschi, J., and T. F. Stocker, 2002: Rapid changes of the oceanic circulation in a hierarchy of ocean models. *Tellus,* **54A,** 273–287.

Huck, T., and G. K. Vallis, 2001: Linear stability of the three-dimensional thermally driven ocean circulation: Application to interdecadal oscillations. *Tellus,* **53A,** 526–545.

Knutti, R., and T. F. Stocker, 2002: Limited predictability of the future thermohaline circulation close to an instability threshold. *J. Climate,* **15,** 179–186.

——, ——, and D. G. Wright, 2000: The effects of subgrid-scale parameterizations in a zonally averaged ocean model. *J. Phys. Oceanogr.,* **30,** 2738–2752.

Kuhlbrodt, T., A. Griesel, M. Montoya, A. Levermann, M. Hofmann, and S. Rahmstorf, 2007: On the driving processes of the Atlantic meridional overturning circulation. *Rev. Geophys.,* **45,** RG2001, doi:10.1029/2004RG000166.

Levitus, S., 1982: *Climatological Atlas of the World Ocean*. NOAA Prof. Paper 13, 173 pp and 17 microfiche.

Lohmann, B., and J. Schneider, 1999: Dynamics and predictability of Stommel's box model: A phase-space perspective with implications for decadal climate variability. *Tellus,* **51A,** 326–336.

Manabe, S., and R. J. Stouffer, 1999: Are two modes of thermohaline circulation stable? *Tellus,* **51A,** 400–411.

McManus, J., R. Francois, J. M. Gherardi, L. D. Keigwin, and S. Brown-Leger, 2004: Collapse and rapid resumption of Atlantic meridional circulation linked to deglacial climate changes. *Nature,* **428,** 834–837.

Meehl, G. A., and Coauthors, 2007: Global climate change projections. *Climate Change 2007: The Physical Science Basis,* S. Solomon et al., Eds., Cambridge University Press, 747–846.

Monahan, A. H., J. Alexander, and A. J. Weaver, 2008: Stochastic models of the meridional overturning circulation: Time scales and patterns of variability. *Philos. Trans. Roy. Soc. London,* **366A,** 2527–2544.

Moore, A. M., C. L. Perez, and J. Zavala-Garay, 2002: A non-normal view of the wind-driven ocean circulation. *J. Phys. Oceanogr.,* **32,** 2681–2705.

——, J. Vialard, A. T. Weaver, D. L. T. Anderson, R. Kleeman, and J. R. Johnson, 2003: The role of air–sea interaction in controlling the optimal perturbations of low-frequency tropical coupled ocean–atmosphere modes. *J. Climate,* **16,** 951–968.

O'Hare, G., A. Johnson, and R. Pope, 2005: Current shifts in abrupt climate change: The stability of the North Atlantic conveyor and its influence on future climate. *Geography,* **90,** 250–266.

Pasquero, C., and E. Tziperman, 2004: Effects of a wind-driven gyre on thermohaline circulation variability. *J. Phys. Oceanogr.,* **34,** 805–816.

Pedlosky, J., 1987: *Geophysical Fluid Dynamics*. Springer-Verlag, 624 pp.

Rahmstorf, S., 2002: Ocean circulation and climate during the past 120,000 years. *Nature,* **419,** 207–214.

Schmidt, G., and L. Mysak, 1996: The stability of a zonally averaged thermohaline circulation model. *Tellus,* **48A,** 158–178.

Schmittner, A., and T. F. Stocker, 1999: The stability of the thermohaline circulation in global warming experiments. *J. Climate,* **12,** 1117–1133.

——, and ——, 2001: A seasonally forced ocean–atmosphere model for paleoclimate studies. *J. Climate,* **14,** 1055–1068.

——, and A. J. Weaver, 2001: Dependence of multiple climate states on ocean mixing parameters. *Geophys. Res. Lett.,* **28,** 1027–1030.

Sevellec, F., M. B. Jelloul, and T. Huck, 2007: Optimal surface salinity perturbations influencing the thermohaline circulation. *J. Phys. Oceanogr.,* **37,** 2789–2808.

Stocker, T. F., and D. G. Wright, 1991: Rapid transitions of the ocean's deep circulation induced by changes in surface water fluxes. *Nature,* **351,** 729–732.

——, and ——, 1996: Rapid changes in ocean circulation and atmospheric radiocarbon. *Paleoceanography,* **11,** 773–795.

——, ——, and W. S. Broecker, 1992a: The influence of high-latitude surface forcing on the global thermohaline circulation. *Paleoceanography,* **7,** 529–541.

——, ——, and L. A. Mysak, 1992b: A zonally averaged, coupled ocean–atmosphere model for paleoclimate studies. *J. Climate,* **5,** 773–797.

——, W. S. Broecker, and D. G. Wright, 1994: Carbon uptake experiments with a zonally-averaged global ocean circulation model. *Tellus,* **46B,** 103–122.

Stommel, H., 1961: Thermohaline convection with two stable regimes of flow. *Tellus,* **13,** 224–230.

Trefethen, L. N., 1997: Pseudospectra of linear operators. *SIAM Rev.,* **39,** 383–406.

Tziperman, E., 1997: Inherently unstable climate behaviour due to weak thermohaline ocean circulation. *Nature,* **386,** 592–595.

——, and P. J. Ioannou, 2002: Transient growth and optimal excitation of thermohaline variability. *J. Phys. Oceanogr.,* **32,** 3427–3435.

——, L. Zanna, and C. Penland, 2008: Nonnormal thermohaline circulation dynamics in a coupled ocean–atmosphere GCM. *J. Phys. Oceanogr.,* **38,** 588–604.

Vellinga, M., 1996: Instability of two-dimensional thermohaline circulation. *J. Phys. Oceanogr.,* **26,** 305–319.

——, and R. A. Wood, 2002: Global climatic impacts of a collapse of the Atlantic thermohaline circulation. *Climatic Change,* **54,** 251–257.

Weaver, A., C. Bitz, A. Fanning, and M. Holland, 1999: Thermohaline circulation: High-latitude phenomena and the difference between the Pacific and Atlantic. *Annu. Rev.,* **27,** 231–285.

Wright, D. G., and T. F. Stocker, 1991: A zonally averaged ocean model for the thermohaline circulation. Part I: Model development and flow dynamics. *J. Phys. Oceanogr.,* **21,** 1713–1724.

——, and ——, 1992: Sensitivities of a zonally averaged global ocean circulation model. *J. Geophys. Res.,* **97,** 12 707–12 730.

——, C. B. Vreugdenhil, and T. M. C. Hughes, 1995: Notes and correspondence: Vorticity dynamics and zonally averaged ocean circulation models. *J. Phys. Oceanogr.,* **25,** 2141–2154.

Zanna, L., and E. Tziperman, 2005: Nonnormal amplification of the thermohaline circulation. *J. Phys. Oceanogr.,* **35,** 1593–1605.

——, and ——, 2008: Optimal surface excitation of the thermohaline circulation. *J. Phys. Oceanogr.,* **38,** 1820–1830.